Microsc. Microanal. 19, 1698–1708, 2013
doi:10.1017/S1431927613012695

Microscopy AND Microanalysis

Low-Voltage Electron-Probe Microanalysis of Fe–Si Compounds Using Soft X-Rays

Phillip Gopon,[1,*] John Fournelle,[1] Peter E. Sobol,[1] and Xavier Llovet[2]

[1]*Department of Geoscience, University of Wisconsin, Madison, WI 53706, USA*
[2]*CCiTUB, University of Barcelona, ES-08028 Barcelona, Spain*

Abstract: Conventional electron-probe microanalysis has an X-ray analytical spatial resolution on the order of 1–4 μm width/depth. Many of the naturally occurring Fe–Si compounds analyzed in this study are smaller than 1 μm in size, requiring the use of lower accelerating potentials and nonstandard X-ray lines for analysis. Problems with the use of low-energy X-ray lines (soft X-rays) of iron for quantitative analyses are discussed and a review is given of the alternative X-ray lines that may be used for iron at or below 5 keV (i.e., accelerating voltage that allows analysis of areas of interest <1 μm). Problems include increased sensitivity to surface effects for soft X-rays, peak shifts (induced by chemical bonding, differential self-absorption, and/or buildup of carbon contamination), uncertainties in the mass attenuation coefficient for X-ray lines near absorption edges, and issues with spectral resolution and count rates from the available Bragg diffractors. In addition to the results from the traditionally used Fe Lα line, alternative approaches, utilizing Fe Lβ, and Fe Ll-η lines, are discussed.

Key words: soft X-ray, low voltage, nanoanalysis, microprobe, EPMA

Introduction

Conventional electron-probe microanalysis (EPMA) uses high electron beam energies (15–20 keV) to eject inner shell electrons and measures the characteristic photon energy emitted when an outer shell electron transitions into the vacant inner shell electron state. The sample volume excited by a 15–20 keV electron beam is generally on the order of several cubic microns (depending on the material's density and the electron beam energy used) and is therefore not suited for analyses of most features under 2-μm width (Fig. 1). With samples under $\sim$2 μm, the electron beam may cause primary ionization of atoms outside the feature of interest. To properly analyze most samples under 2 μm, low-voltage (at or below 5 keV) electron beams must be used. However, when using lower electron beam energies, many of the inner shell electrons that are generally used in EPMA (i.e., Fe K-shell) can no longer be ionized. The outer shell electrons (e.g., L or M) used at low keV result in the possibility that the electrons involved might be strongly affected by bonding environment differences between a standard and unknown.

In the past, there has been little interest in quantitative low-voltage EPMA because with older tungsten source instruments the electron beam cannot be focused at low voltage to the small diameters required. LaB_6 sources provided tighter beams but have issues due to probe current drift. The new generation of field emission electron probes that allow for submicron beam focusing at low keV make it more pressing to understand the as yet poorly studied L and M lines that will be necessary for low accelerating voltage EPMA.

Received November 26, 2012; accepted June 7, 2013
*Corresponding author. E-mail: pgopon@geology.wisc.edu

A recent study (Llovet et al., 2012) showed the difficulties of using L lines for quantitative EPMA. Some of the causes of these problems include changes in peak position/shape of the X-ray lines, increased sensitivity to surface contamination, and errors in the accuracy of the tabulated mass attenuation coefficients (MACs) for low-energy X-rays. The Lα lines of the first-row transition metals are particularly problematic for quantitative analysis due to proximity to their respective L_3 absorption edges. Note that the Lα line is actually the unresolvable combination of the Lα_1 and Lα_2 transitions, and is therefore simply referred to as Lα in this article (rather than the more correct but cumbersome L$\alpha_{1,2}$). The Lβ transition discussed later is simply the Lβ_1 transition.

Fournelle (2011, unpublished data) attempted to determine the compositions of both small samples of lunar Fe–Si compounds (Fig. 2) and then larger samples of commercial Fe–Si compounds. Those experimental EPMA results at 5 keV using pure Si and Fe standards and the Fe Lα line with a PC1 (pseudocrystal) diffracting crystal (60 Å W–Si) resulted in extremely high measured iron concentrations (i.e., over 20 wt% greater than nominal Fe wt%, with $>$120 wt% totals; Table 1). He noted that the K-ratio (counts on the unknown divided by counts on the standard) for the Fe Lα was apparently much higher ($\sim$133% high for Fe–Si) than would be predicted by Castaing's first approximation (Castaing, 1951).

The motivation for the current study was an attempt at a proper EPMA analysis on submicron lunar Fe–Si compounds reported by Spicuzza et al. (2011) in Apollo 16 lunar regolith (Fig. 2). These are hypothesized to have formed in the reducing environment of the moon after micrometeorite impacts (Anand et al., 2004). Iron silicides have been reported elsewhere in lunar regolith (Anand et al., 2004; Spicuzza et al., 2011), as well as in terrestrial (lightning-induced) fulgarites (Essene & Fisher, 1986), and Stardust

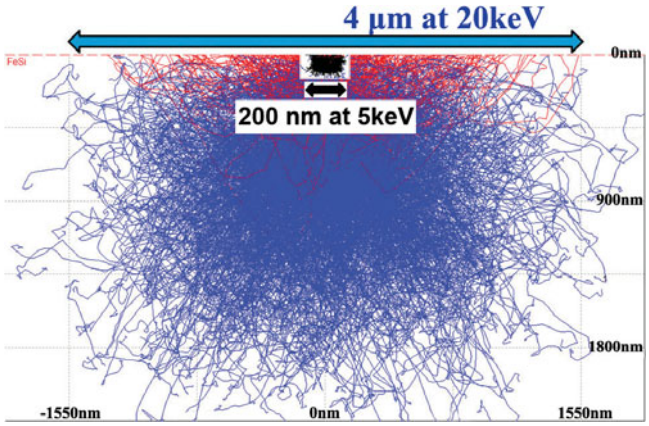

Figure 1. Monte Carlo simulation of the interaction volumes of a 5 keV (black) and 20 keV (blue) incident electron beam in FeSi (using CASINO software; Drouin et al., 2007).

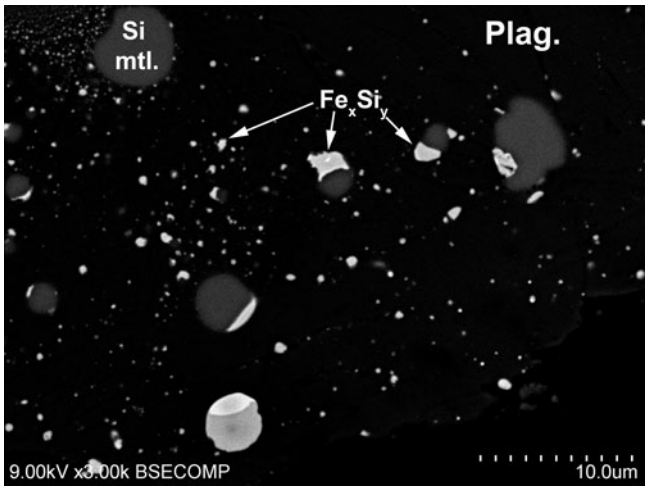

Figure 2. Backscattered electron image of plagioclase grain A6-8 from Apollo 16 lunar regolith showing micro/nanophase Fe–Si compounds (bright phases), in plagioclase matrix, the medium bright phases are silicon metal.

samples (Rietmeijer et al., 2008). They are significant because of the extreme reducing conditions required for formation; however, their small size (<1 μm) precludes quantitative measurements using conventional EPMA.

The objectives of this study are to advance the techniques for soft X-ray EPMA and ultimately to be able to perform quantitative analyses on submicron phases (i.e., the lunar Fe–Si). Unlike the alloy steels studied by Llovet et al. (2012), the Fe–Si system is particularly well suited for the latter goal, because it involves only two elements. The inner shell transition Si Kα line is still excited by a low keV incident electron beam, allowing for focusing on the problem of the outer shell Fe L lines. Also, a relatively large suite of possible Fe–Si phases exists on which to conduct analyses (Fig. 3).

Use of Fe L Lines in EPMA

Interest in Fe L lines is not new in EPMA. Early interest focused upon changes in peak shape and position between Fe metal and Fe oxides (Fischer & Baun, 1967). Anderson (1967) in a review of soft X-ray EPMA, included a study of the use of three Fe L lines: Fe Lα, Fe Lβ, and Fe Ll. He used pure Fe and Fe_3O_4 standards to quantify the Fe in two Fe oxides, FeS_2 and Fe_3C, and noted major problems. O'Nions & Smith (1971) evaluated Fe Lα–Lβ spectra of a variety of minerals with different oxidation states in the hope of using EPMA to easily determine Fe^{3+}/Fe^{2+} ratios. The results were not encouraging. All of these studies refer to the issue of carbon contamination and of surface artifacts having a deleterious role. They have ranged from describing the detailed electron structure of iron compounds to being able to determine the ferrous to ferric iron ratio in minerals of interest to geologists.

Fialin et al. (2001) described methods to determine the ferrous to ferric iron ratios in materials. It was found that there was a correlation between the iron oxidation state and the Fe Lα peak position. Another method they described used the ratio of the heights of the Fe Lα and Lβ peaks to determine oxidation states. This article provides significant insight into the changes in the Fe Lα/β positions, shapes, and heights with oxidation state.

Höfer and Brey (2007) attempted to determine the oxidation state of iron in garnets. They were able to determine $Fe^{3+}/\Sigma Fe$ ratios of garnets to within $\sim$0.05, compared to Mössbauser results. Ohnuma et al. (2012) conducted a study of nanophase Fe–Si compounds using a field emission electron probe. Their study, however, did not address the issue being considered here, which is the fundamental problem behind the inability to utilize elemental standards for these intermetallic compounds. They applied the well-known and proven technique of "using standards similar to the unknown," using a bulk alloy of similar composition to a limited region of the Fe-rich end of the Fe–Si phase diagram.

Studies describing the changing electron properties of iron essentially provide insight into spectroscopic problems of using the Fe L lines. Fewer studies have been conducted where the Fe L lines are used strictly for quantitative EPMA (spectrometry). Llovet et al. (2012) conducted an interlaboratory study to show the problems inherent in using L lines of the first row transition metals for quantitative EPMA. This study used homogenous alloy steel samples as the "known unknowns." Generally, the participating laboratories obtained erroneous concentrations of the major elements Fe, Cr, and Ni, using Lα lines. In an interesting approach, Armstrong (2011) avoided the analytical conundrum of the Fe Lα line by using 8-keV-beam energy, exciting the Fe–K line at low overvoltage. As the incident electrons interact with the sample they lose energy rapidly, meaning that with low overvoltage the electrons do not have enough energy to excite the Fe Kα line after interaction with the sample surface, yielding typically very low count rates. Low overvoltage yields smaller excitation volumes for the Fe Kα line compared to the low energy Si Kα line. This leads to two separate analytical volumes for Fe and Si, where the Fe volume is small enough for phase of interest, but the Si

Table 1. Comparison of Fe Lα, Lβ, and Ll and the Effect of Different Mass Attenuation Coefficients (MACs) for Quantitative Electron-Probe Microanalysis (EPMA) at 5 keV.*

at.%	wt%	wt% 15 keV		Lα			Lβ			Ll		
			MAC	Fe (wt%)	Si (wt%)	Total (wt%)	Fe (wt%)	Si (wt%)	Total (wt%)	Fe (wt%)	Si (wt%)	Total (wt%)
$Fe_{90}Si_{10}$	$Fe_{94.71}Si_{5.20}$	$Fe_{95.13}Si_{5.23}$	Henke	94.22	4.95	99.17	X	X	X	X	X	X
			Heinr	94.21	4.95	99.16	95.50	5.04	100.53	94.37	4.99	99.36
			Chant	94.26	4.95	99.21	95.89	5.04	100.92	94.33	4.95	99.28
			Sokar	93.87	4.95	98.82	95.64	5.04	100.68	X	X	X
			Gopon	93.86	4.95	98.81	94.80	5.04	99.84	X	X	X
$Fe_{75}Si_{25}$	$Fe_{85.64}Si_{14.36}$	$Fe_{85.08}Si_{13.34}$	Henke	93.16	13.85	107.02	X	X	X	X	X	X
			Heinr	93.16	13.85	107.01	87.76	14.26	102.02	86.14	13.99	100.13
			Chant	93.27	13.85	107.13	88.81	14.26	103.07	86.01	13.87	99.88
			Sokar	92.28	13.85	106.13	88.15	14.26	102.42	X	X	X
			Gopon	92.27	13.85	106.12	85.84	14.26	100.11	X	X	X
$Fe_{70}Si_{30}$	$Fe_{82.27}Si_{17.73}$	$Fe_{82.97}Si_{16.34}$	Henke	93.97	17.03	111.01	X	X	X	X	X	X
			Heinr	93.97	17.03	111.00	88.94	18.22	107.16	83.25	17.21	100.46
			Chant	94.11	17.03	111.14	90.26	18.22	108.48	83.11	17.07	100.18
			Sokar.	92.92	17.04	109.96	89.44	18.22	107.66	X	X	X
			Gopon	92.91	17.04	109.95	86.53	18.22	104.75	X	X	X
$Fe_{50}Si_{50}$	$Fe_{66.54}Si_{33.46}$	$Fe_{67.23}Si_{31.21}$	Henke	86.80	32.99	119.79	X	X	X	X	X	X
			Heinr	86.79	32.99	119.78	74.25	34.40	108.65	67.57	33.45	101.02
			Chant	87.01	32.99	120.00	76.45	34.39	110.85	67.37	33.22	100.59
			Sokar	85.11	33.01	118.12	75.08	34.40	109.48	X	X	X
			Gopon	85.09	33.01	118.10	70.09	34.42	104.51	X	X	X
$Fe_{33}Si_{67}$	$Fe_{49.82}Si_{50.18}$	$Fe_{47.35}Si_{50.17}$	Henke	66.88	52.51	119.39	X	X	X	X	X	X
			Heinr	66.86	52.51	119.38	54.47	53.93	108.41	47.41	53.31	100.72
			Chant	67.13	52.51	119.64	57.23	53.90	111.13	47.23	53.06	100.29
			Sokar	64.85	52.56	117.41	55.53	53.92	109.44	X	X	X
			Gopon	64.83	52.56	117.39	49.25	54.00	103.25	X	X	X
$Fe_{30}Si_{70}$	$Fe_{46.01}Si_{53.99}$	$Fe_{44.67}Si_{53.66}$	Henke	61.96	55.96	117.92	X	X	X	X	X	X
			Heinr	61.94	55.96	117.90	47.86	56.57	104.43	43.62	56.78	100.40
			Chant	62.21	55.96	118.17	50.54	56.53	107.06	43.45	56.54	99.99
			Sokar	59.94	56.02	115.96	50.36	57.25	107.60	X	X	X
			Gopon	59.53	56.02	115.55	42.79	56.65	99.44	X	X	X

*Fe Lα and Lβ were acquired and quantified in Probe for EPMA, using the full PAP matrix correction. Fe Ll was acquired in Probe for EPMA, but quantified in DTSA II using the full PAP matrix correction. The Ll data only shows results for Heinrich and Chantler because DTSA II only allows for use of those two MAC tables. At the top of each composition (black background) is both the nominal composition of the phase (left), and the composition as measured at 15 keV (right) using the Fe Kα line with the LIF crystal, the PAP matrix correction, and the Chantler MACs. All data were acquired on the platinum-coated Fe–Si standards block shown in Figure 6, with the exception of the 15 keV data, which was acquired in the same block when it had a carbon coating.

volume is larger than needed, which is not optimal if submicron features are being analyzed, particularly if the sample sits in a matrix containing Si, as is the case in the lunar iron silicides.

MACs

Part of our study focuses on the use and determinations of MACs, which can reach large values (e.g., 14,400 cm^2/g for absorption of Fe Lβ by Fe) for low-energy X-rays in certain materials. Historically, MACs were first and most easily determined for gases, with theories developed and fits created to the sparse experimental data. For a given (absorber) element, MACs are plotted from low to high energies, with specific energies that pertain to given X-ray lines plotted in tables. In general, MACs slowly and gradually decrease until the vicinity of an edge, where there is a rapid increase, a region of variability, then another gradual decrease until the next edge is reached. Henke et al. (1957) showed that for "many" line/matrix combinations, one could get within 2.4% error of the empirical data simply by using the universal function $\mu/\rho = N_o \sum \tau/A$ for the regions between, and away from, the edges; where N_o is Avagadro's number, τ is the total photoelectric cross section for the shell of interest, and A is the atomic weight. This universal function and other algorithms do not properly predict MACs near absorption edges, a fact that has been reiterated many times in the

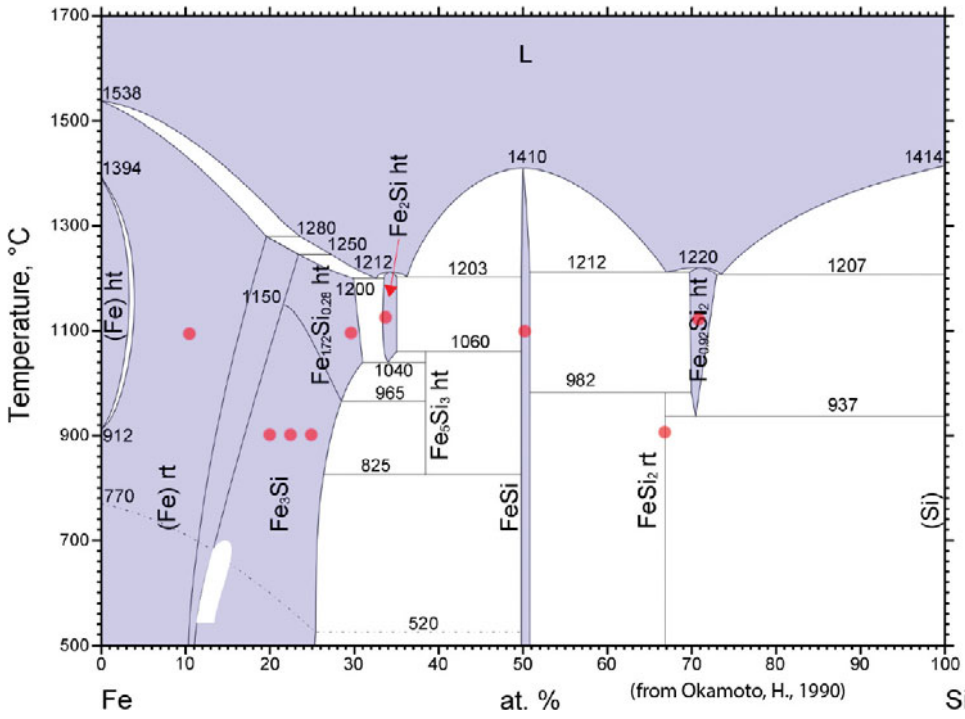

Figure 3. Phase diagram of the Fe–Si binary system, with the samples synthesized for this study marked in red. Location of red dot marks both the composition of the phase, as well as the temperature used to anneal it. Purple shaded areas denote single-phase fields, and white shaded areas are two-phase fields.

past (Henke et al., 1957; Heinrich, 1966; Kerur et al., 1993). Kerur et al. (1993) showed that for an X-ray near an absorption edge, there was an 11% error in the compound MAC (and this was a K edge). This may also be involved in the case of Fe silicides where analytical lines may be very close to a critical edge.

If X-ray lines near absorption edges are to be used for quantitative analysis, careful empirical determinations of the MACs are necessary. These experimental determinations of the MAC are difficult to make, particularly because of the difficulties of sample preparation, as the samples need to be 1–5 nm thick. It is therefore very fortuitous for this study that Sokaras et al. (2011) determined the MAC for Fe using two techniques: proton-induced X-ray beams and synchrotron radiation, particularly in high detail in the region of the L edges. Their results differed from previously published values by up to ~40% near absorption edges (Table 2). Note that they examined one material only: pure Fe.

Pouchou (1996) presented a procedure for determining MAC values from EPMA measurements. The method consists of measuring the variation of the X-ray intensity (in counts/s/nA) as a function of the accelerating voltage, on a sample of known composition and then processing the measured X-ray intensities with the help of the program XMAC. This program determines the MAC for the X-ray line of interest by least square fitting the theoretical X-ray intensities calculated with the XPP model to the experimental data (Pouchou et al., 1990). An assumption is that the MAC of any other element present be known accurately. The program is commercially available through SAMX in France.

Finally, in an article by Deslattes (1969) on MACs, in an endpaper comment, Milledge provides a sobering view: "In

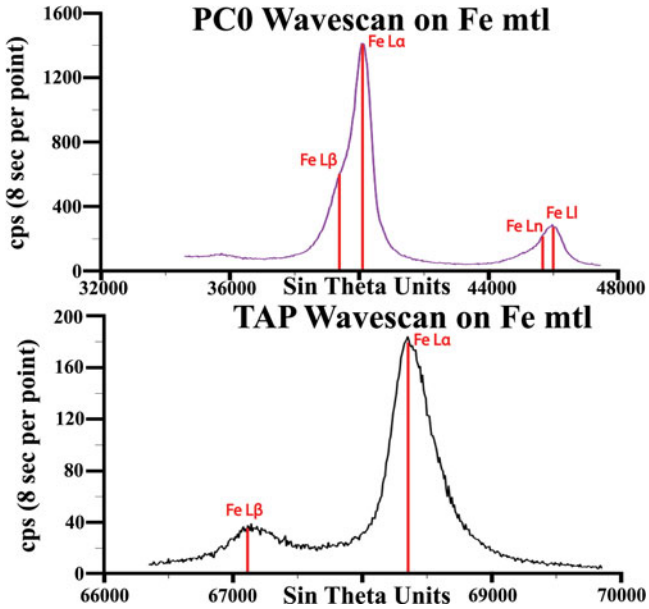

Figure 4. Wavescans on Fe metal using the PC0 (top) and TAP (bottom) crystals. Note the low count rates on the TAP crystal, as well as that Fe Lα and Lβ cannot be resolved on the PC0 crystal.

Table 2. Reported MAC Values (in cm^2/g) from Various Studies.*

Study	Fe Ll by Fe MAC	Fe Lα by Fe MAC	Fe Lβ by Fe MAC
Henke et al. (1982)	NA	2,146	NA
Heinrich (1987)	3,735	2,157	14,400
Chantler et al. (2005)	2,765	1,964	12,093
Sokaras et al. (2011)	2,957	3,626	~13,500
Gopon et al. (2012)	3,162	3,639	19,500

*Note the variation in numbers between the studies.

preparing the values for the *International Tables* [absorption factors], we decided to put the less reliable in italics—perhaps we should have put them all in italics. The trouble was that there just were not enough experimental values."

Materials and Methods

Analyses were first conducted at the Eugene Cameron Electron Microprobe Laboratory (UW, Madison) using a CAMECA SX-51 electron microprobe (W-filament source, operated at 5 keV) and Probe for EPMA software (Donovan et al., 2012). Initial data obtained on the Fe–Si reference materials (mounted in epoxy and coated with an ~200 Å carbon coating) using the Fe Lα, and Si Kα lines returned ~120 wt% totals. In each case the Fe wt% was anomalously ~20 wt% high. In all cases we used the same high purity metals as standards (99.99% Fe and 99.9% Si). The metal standards were mounted in each Fe–Si block. To validate the high wt% totals, a sample mount with the Fe–Si reference materials was sent to the University of Barcelona to be analyzed on a CAMECA SX-50. Also, the reference materials, as well as the lunar grain, were analyzed on the prototype CAMECA SX-5 FE, located in Fitchburg, WI, at the time. Similar erroneous results were obtained on all machines.

Our approach was to obtain several Fe silicides of well-determined compositions, then study the possible factors involved in the inaccurate Fe compositional determinations, initially focusing on (1) chemical peak shifts, (2) comparing usage of the three possible crystal diffractors: TAP, PC0 (45 Å W–Si), PC1 (count rates versus spectral resolution), and (3) MACs.

The Fe Lα line was used with a 5 keV (20 nA) primary beam and the TAP crystals to test the degree of the problems when using this line. The TAP crystal was selected as it is the only crystal that is able to resolve the Fe Lα and Lβ line, even though it has low counts compared to the layered diffracting elements/pseudocrystals (LDE/PC; Fig. 4). The lower count rates required high current (100 nA) primary beams resulting in complications from carbon contamination.

The Fe–Si samples had to be large enough to be analyzed with a tungsten source. Some were supplied by a colleague (E. Heikinheimo, Aalto University, Espoo, Finland). Others were synthesized in the UW-Madison Departments of Material Science and Chemistry. Fe:Si ratios in the synthetic samples were chosen to ensure that the full range of compositions in the Fe–Si system were covered. Samples were first weighed as a powder, using reagent grade material, then pressed into pellets. The pellets were then transferred to an arc melter, where the samples were arc melted three times. The entire procedure (weighing, pressing, and arc melting) was carried out in an argon-filled glove box to minimize oxidation.

Multiple samples of each phase were synthesized. The samples were annealed at either 900 or 1,125°C for a month at a time until each sample was deemed fully homogenous (Fig. 5). After each month of annealing one of the samples from each phase was quenched, cut in half, and checked with high-contrast backscattered electron imaging (on a Hitachi S3400-N scanning electron microscope) to verify phase homogeneity. The reference materials were then analyzed with the UW Madison CAMECA SX-51 at 15 keV to determine the composition of the reference materials, as there is some solid solution in some of the phase fields.

For EPMA the synthesized samples were mounted in either epoxy or polished as individual grains and pressed

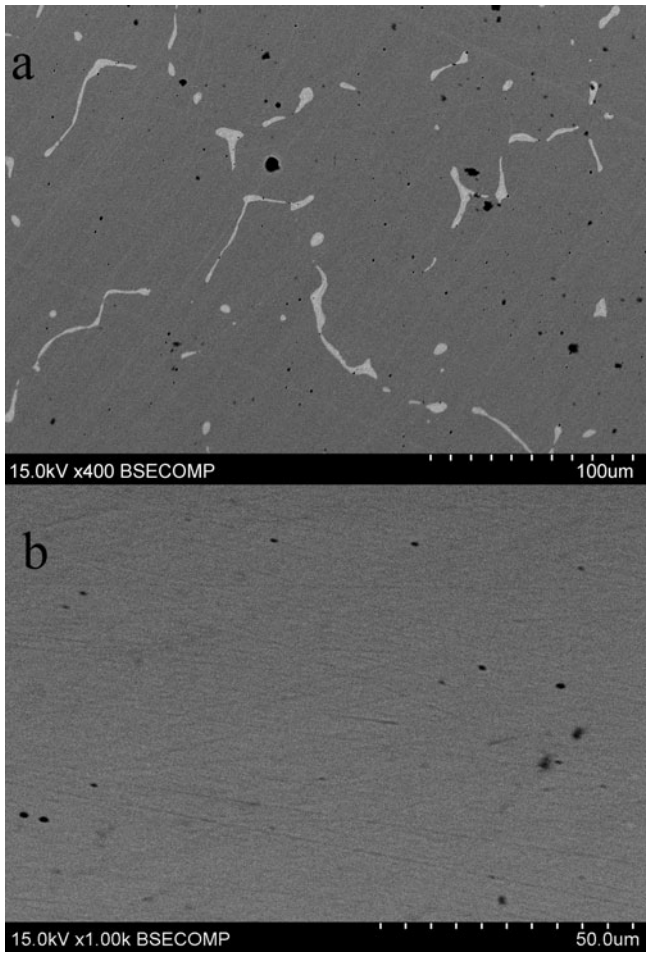

Figure 5. Backscattered electron images of FeSi after 1 week (**a**) and 4 weeks (**b**) annealing at 1,100°C.

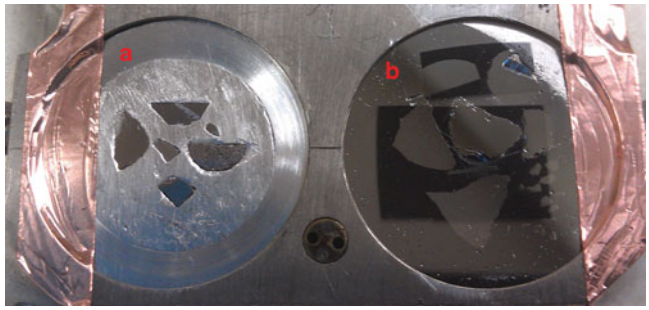

Figure 6. **a**: Indium-mounted synthetic Fe–Si samples. Sample left uncoated. **b**: Platinum-coated synthetic Fe–Si samples mounted in epoxy. The edges are coated with 30 nm of Pt to maximize conduction, while the samples are coated with 1.03 nm Pt.

into indium due to concern of carbon contamination (Fig. 6). The epoxy mount was polished using a series of Buehler diamond suspensions, with a final colloidal silica or alumina polishing stage. The indium pressed samples were individually polished on a diamond lapping film with 0.1 μm as the final polish. The samples were pressed into the indium mount with a vice and a glass slide as a cover. Two epoxy mounts were made with the same samples and polished in the same manner. One of the epoxy mounts was coated with 200 Å of carbon and the second epoxy mount was coated with 10.3 Å of platinum. The indium mount was left uncoated, as both the Fe–Si sample and the indium are conductive.

Long duration scans of the Fe L peaks (~1.5 h each; 200 channels, 20 s/channel) were obtained on each of the compounds and interpreted for peak shifts. It was noted that there was a potential problem with long wavescans of soft X-ray lines, due to the increased time that a carbon contamination spot could develop. One anti-contamination measure used was the CAMECA anti-contamination device, a liquid nitrogen-cooled plate over the diffusion pump as well as a liquid nitrogen cold finger. However, it was decided not to use the "air jet" measure as it was observed that oxidation readily occurs on the synthetic samples (Fialin et al., 1998).

In evaluating the scans, a concern arose that the buildup of carbon contamination during the hour-long dwell at a single point might have some impact on the peak shape. Initially, this concern led to first reversing the direction of the spectrometer scan. Comparisons confirmed that the carbon buildup was causing an apparent peak shift (Gopon et al., 2013). Subsequently, a program was developed that allows the movement of the spectrometer across the range of the wavescan in a random sequence to eliminate the systematic relationship between time and crystal position. With these random sequence acquisitions, a predetermined evenly spaced set of points within the range of the wavescan are run in a random order.

To test the trend in the rate of accumulation (and how to correct for it), a series of experiments on the epoxy mounted Fe silicides was conducted in which Fe Lα, Si Kα, and C Kα intensities were counted every 10 s over the course of an hour. The rate of carbon accumulation was tested using 20, 51, and 100 nA. These experiments were repeated on the Fe–Si reference materials that were pressed into indium and left carbon-uncoated to minimize the effect of the carbon coating and carbon contamination in the chamber. It was found that on a carbon-uncoated sample the rate of accumulation for the carbon contamination spot was lowest at 100 nA.

The Fe–Si reference materials in the indium mount were then quantitatively analyzed using 5 keV/100 nA using both the Fe Lα and Lβ lines on the indium-mounted samples. By analyzing an uncoated sample at 100 nA with short count times (20 s on peak/10 s on the background) we avoided most of the time-dependent effects of the carbon buildup. Alternatively, a time-dependent intensity (TDI) correction, such as that used in the Probe for EPMA software (Donovan et al., 2012) could be used; however, it was not needed in the case of our analyses because of the care taken to avoid carbon-coated samples. The iron wt% was closer to the nominal composition, but still high (Table 1).

Fialin et al. (1998) suggested the use of Ll and Lη lines, as alternatives to the normally used Lα and Lβ lines. As none of the commercially available electron probe software allows for the use of Ll-η lines for quantitative analysis, an alternative method was used to test the feasibility of the Fe Ll line for quantitative EPMA. The raw counts were obtained on the UW Madison CAMECA-SX 51, using the Probe for EPMA software, and "mispeaking" the Fe Lα line on the Ll line. The K-ratios obtained were then run through the Pouchou and Pichoir model (Pouchou & Pichoir, 1984) matrix corrections in "Son of Desktop Spectrum Analyzer" (DTSA II; Ritchie, 2009). The quantification tool in DTSA II does not allow for use of Ll lines; however, in the newest version of the software (Gemini), a command window is available for implementing a desired code. Phillippe Pinard at RTWH Aachen (Germany), wrote a script for DTSA II that allowed the quantification of Ll lines. This code was then used to determine the compositions of our Fe–Si compounds, with the K-ratios determined in Probe for EPMA.

A choice needs to be made as to which diffracting crystal to use for the Fe Ll peak: the higher resolution TAP (with very low counts and requiring high-beam currents, thereby inducing carbon contamination) or instead the synthetic LDE PC0–PC1 (45–60 Å 2d spacing) which have significantly higher count rates (the PC1 crystal having the highest counts). In the latter case, lower beam currents may be used and the issue of carbon contamination lessened. However, with the LDE the Ll and Lη peaks overlap. This does not seem to be a significant detriment to this procedure (and actually enhances the counting statistics).

Results and Discussion

Surface Contamination Effects

Surface effects (carbon buildup) are generally small for conventional EPMA analyses as they do not develop fast enough in a normal analysis nor are the X-ray lines used affected much by a thin surface layer. However, the low-energy Fe L lines are strongly affected by surface effects. Figure 7 shows the results of sample exposure to a 5-keV-electron beam, at varying currents. Figure 7a shows the results for an Fe–Si sample mounted in epoxy and carbon coated; while Figure 7b shows the results with the same Fe–Si sample pressed into an indium mount and left uncoated. Note in Figure 7a, the initial drop off in carbon counts (and subsequent rise in Si and Fe counts), which is believed to be caused by the electron beam (with sufficient current) locally ablating the carbon coating. After the initial drop off, the carbon contamination spot starts slowly building up in a nonlinear fashion, with the Si and Fe counts slowly dropping as the C increases. The rate of

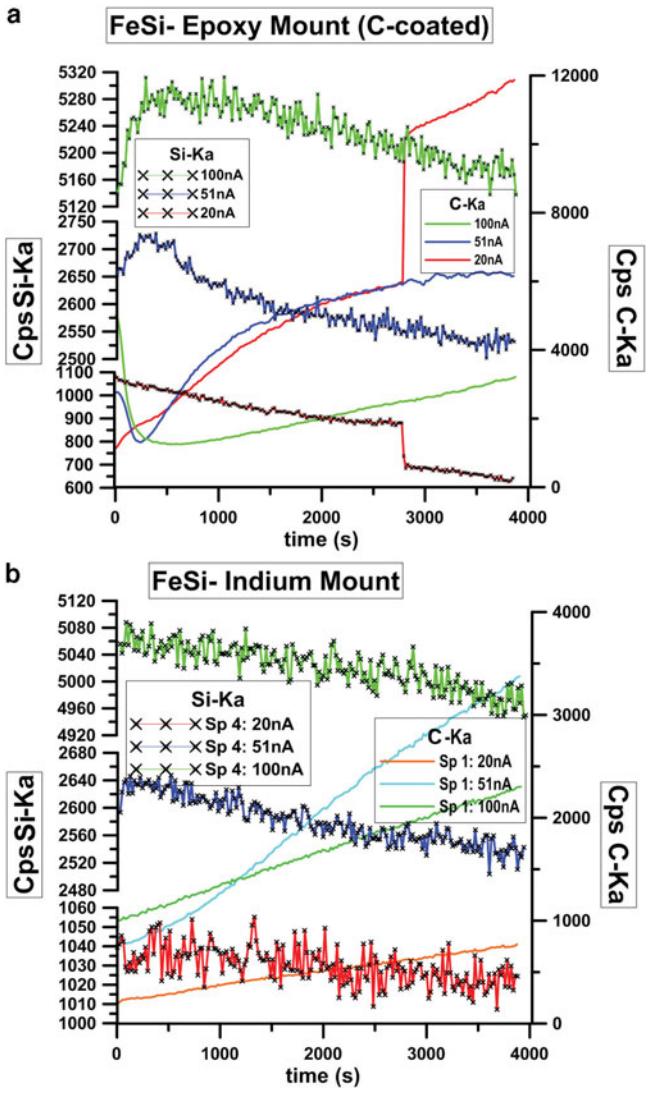

Figure 7. Time-dependent variation of Si Kα counts on FeSi in a carbon-coated epoxy mount (**a**), and an uncoated indium mount (**b**) for three different currents (all at 5 keV). The left scale bar (and the data with black ×s) is raw unbackground corrected Si Kα cps, while the right scale bar (and the data without the black ×s) is raw unbackground corrected C Kα cps. The sample colored lines correspond to the same current, so the Si and C counts were acquired at the same time. Note that as the C counts go down the Si counts go up, and vice versa.

carbon accumulation after the initial drop off is actually lowest for the experiment at 100 nA. Note that during the 20 nA experiment there was an unexpected (and nonreproducible) sharp increase in the C contamination possibly due to the stage or beam inadvertently moving a micron andtransferring the beam to a higher point on the "carbon volcano," and there is a corresponding drop in the Si and Fe counts.

A potential solution to the changing counts is to use the TDI feature of the Probe for EPMA software, to correct for the local ablation of the carbon coating. Alternatively, this initial drop off in carbon counts does not occur with the uncoated indium pressed sample (Fig. 7a), and the rate of carbon accumulation is also slower than for the epoxy

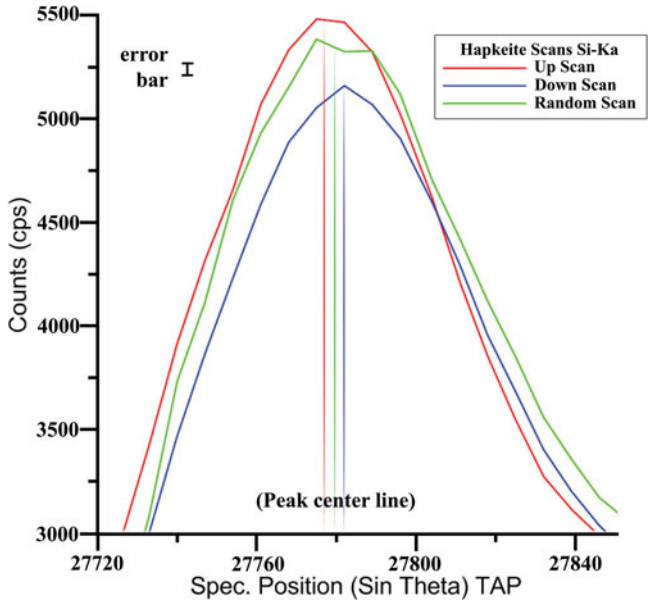

Figure 8. Carbon-induced apparent peak shifts. Here for long wavescans (1h) at high current (100 nA, 5 keV) the peak appears to be shifted in the opposite direction of the spectrometer motion used to acquire the wavescan. When the spectrometer is moved from low to high sin θ, the peak is shifted to lower sin θ. The green wavescan is acquired with random spectrometer motion, to remove the time dependency of the carbon contamination spot. Spectrometer motor backlash would account for a peak shift in the direction of the scan, not in the opposite direction as is shown in the figure.

mount. Again the 100 nA experiment shows the slowest rate of carbon accumulation. The platinum-coated epoxy mount has similar behavior for carbon ablation and accumulation to the uncoated indium mount, and was therefore used for all low-voltage quantitative analyses in this study (unless specifically noted otherwise).

The carbon contamination accumulation and the subsequent drop in Fe and Si counts leads to changing count rates during a quantitative analysis, and leads to apparent carbon-induced peak shifts. Figure 8 shows a magnified area of a longer wavescan (1 h), over the Si Kα peak. The three different wavescans shown represent the same material, the only difference being spectrometer motion used to acquire the wavescan. During the "up" wavescan the spectrometer incrementally moved from low sin θ number to high. The "down" wavescan was acquired with the opposite sense of motion. The up and down wavescans give different peak positions and shapes. The development of the carbon contamination spot results in an apparent peak shift in the opposite direction from which the wavescan was acquired. Time-dependent carbon buildup and associated count-rate decrease causes reduction in the counts on the side of the peak obtained later during the scan. On large enough samples it might be possible to simply move the stage or defocus the beam during the wavescan acquisition, but the current samples were not large or homogenous enough to allow for this.

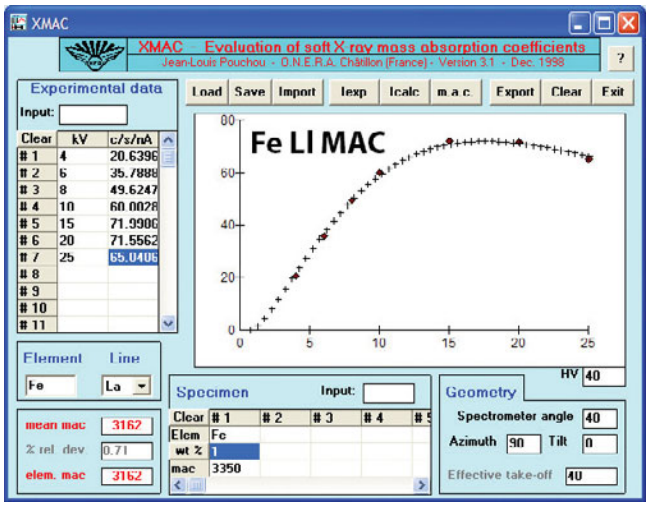

Figure 9. Output window of the XMAC program showing the data collected for the Fe Ll line on FeSi (Pouchou, 1996). Because the XMAC program does not have the option to use Ll lines, the Ll data was input into the program as Fe Lα, which has a similar energy.

Wavescans were also obtained with the previously described random sequence (Gopon et al., 2013) to test the hypothesis that carbon buildup caused apparent peak shifts. The random wavescan finds the center of the peak more accurately than either the up or the down wavescan, and more correctly shows the shape of the peak (Fig. 8). Note that the scatter between any two points is increased, since two points next to each other could have been acquired at the beginning and end of the acquisition. The apparent peak shift cannot be explained by spectrometer motor backlash, because a backlash-induced peak shift would be shifted in the same direction as the motor motion, not the opposite direction as shown in our example.

MACs

A review of the published MACs for the Fe Lα, Lβ, and Ll lines is presented in Table 2, and shows an 85% discrepancy between extremes of the four measurements for Fe Lα especially troubling since the two most recent values show the greatest difference. The Fe Lβ values differ by 19%. We therefore tried to experimentally determine the MACs for these lines using the XMAC program. As mentioned earlier, this program uses a range of accelerating potentials (in the example shown in Fig. 9, seven accelerating voltages were used between 4 and 25 keV). It should be noted that the main assumption of the variable–voltage method is that the underlying X-ray emission model (in this case the XPP model) is error free (Mackenzie, 1993). Therefore, a MAC obtained in this way will in principle be meaningful only when used in conjunction with the same X-ray emission model. The experimentally determined MACs are compared with various published MAC values (for Lα and some Lβ), as well as values for Ll extrapolated from the original curves or formulae (e.g., Chantler et al., 2005; see Table 2).

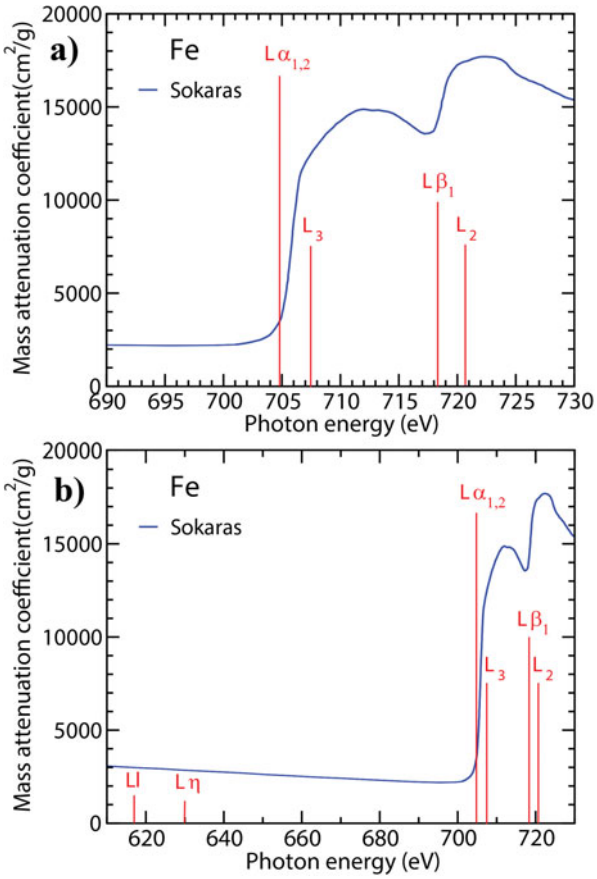

Figure 10. Experimental mass attenuation coefficients (taken from Sokaras et al., 2011) at the energies around the Fe Lα and Lβ lines (**a**) and Fe Lα, Lβ, Ll, and Lη lines (**b**), overlain with the corresponding tabulated line energies, and L_3 and L_2 absorption edges (values taken from Deslattes et al., 2003).

Quantitative Analysis

Table 1 shows the results of using the Fe Lα, Lβ, and Ll lines, as well as different MACs, for the analysis of Fe–Si compounds, at 5 keV. Note that as the Fe content decreases, the error in the Fe value increases for the Fe Lα and Lβ lines. The data with the greatest deviation from the nominal composition is that acquired with the Fe Lα line. The Fe Lβ line gives Fe wt% closer to nominal, but is still off by over 10 wt% for $Fe_{30}Si_{70.}$ The Si wt% obtained at 5 keV are systematically higher than those obtained at 15 keV by a factor ranging from 1.03 to 1.05, except for the $Fe_{90}Si_{10}$ alloy. This discrepancy is probably due to measurement difficulty combined with a change in the matrix correction with the incorrect Fe concentration. The effect of using different MACs is noticeable (~2 wt% difference in Fe counts), but is not enough to correct for the large errors in Fe numbers using the Fe Lα and Lβ lines.

There are at least four phenomena which make spectral work with Fe L X-ray lines challenging. First, the Fe Lα and Lβ lines are close to the L_3 and L_2 absorption edges, respectively. As a result, relatively large changes in the MACs for these lines are observed in the vicinity of the corresponding edges. These changes are originated by near-edge absorption

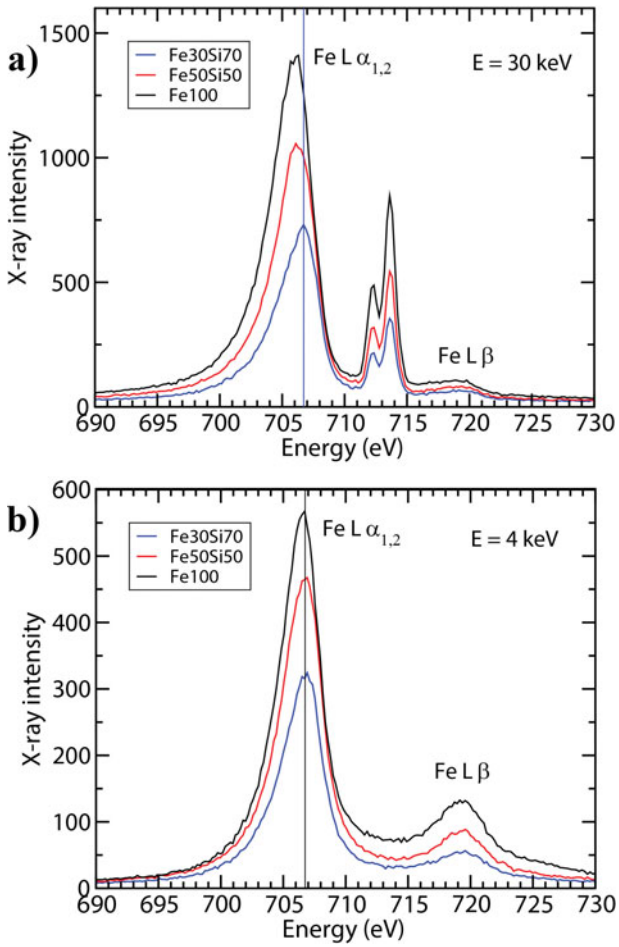

Figure 11. Fe Lα and Lβ emission bands for Fe, $Fe_{30}Si_{70}$ and $Fe_{50}Si_{50}$ measured at 30 keV (**a**) and 4 keV (**b**) electron incident energies. The peaks observed in (**a**) between the Lα and Lβ peaks are the ninth reflection order peaks corresponding to the Kα_1 and Kβ_2 lines. The apparent shifts observed at 30 keV are the result of differential self-absorption.

effects which are produced by molecular or crystalline ordering (Fig. 10) and they are generally ignored in most MAC tabulations. As a result, there may be large uncertainties in the MACs for these lines for Fe–Si compounds as compared to the pure Fe standard. Second, the Lα and Lβ emission lines of Fe are not sharp single channel phenomena, but rather they have a wide natural width (they are actually X-ray bands). Because they lie astride an absorption edge, an enhanced absorption on the high-energy side of the peak shifts the energy position toward lower energy (see Chopra, 1970). This effect is often referred to as "differential" self-absorption. The shift due to differential self-absorption increases with increasing accelerating voltage and/or Fe concentration (in the case of compounds; Fig. 11). Third, the partial filling of the 3*d* electron band in Fe may lead to anomalous X-ray emission and absorption, as described by Pouchou and Pichoir (1984) and Pouchou (1996). Finally, there might also be chemical peak shifts resulting essentially from changes in the electronic structure of the outer orbital electrons due to interactions with different

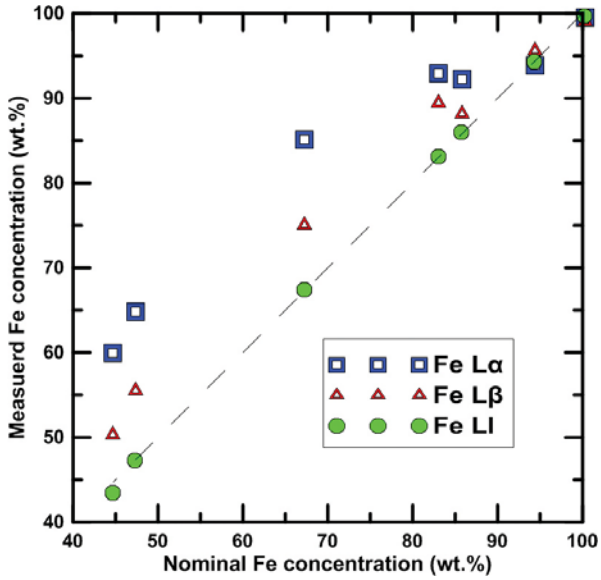

Figure 12. Measured at low voltage versus nominal (as measured at 15 keV with Fe Kα; dashed line) Fe concentrations obtained on the various Fe–Si reference materials, in the epoxy mount coated with platinum (see Fig. 6). Fe Lα and Lβ were acquired and quantified in Probe for EPMA, using the full Pouchou and Pichoir (PAP) matrix correction. Fe Ll was acquired in Probe for EPMA, but quantified in DTSA II using the PAP model.

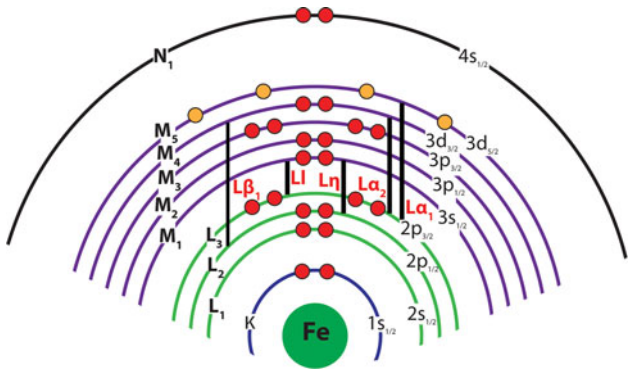

Figure 13. Schematic diagram of Fe electron cloud showing the major X-ray lines in Siegbahn and IUPAC notation, as well as the three transitions, Fe Lα, Lβ, and Ll.

nearest neighbors in a compound (Eisebitt & Rubensson, 1994).

Using the Fe Ll line (L_3–M_1 transition), in conjunction with DTSA II, for quantitative analysis gives compositions closer to the nominal values, even whilst using pure metals as standards. Figure 12 graphically shows the improvement in the measurements, using the various Fe L lines. One possible explanation for the better results obtained by using the Fe Ll line is that this line is the furthest L line away from the L_3 absorption edge (Fig. 10), and unlike the Lβ line, it has a relatively low MAC, and should not be affected by near-edge absorption effects. Moreover, the L_3–M_1 transition involves electron orbitals other than the 3*d* which are not involved in chemical bonding (Fig. 13), thus keeping an "atomic-like" character.

The Fe Ll X-ray lines do not yield high count rates (relative to those of Fe Lα/Lβ). Low count rates mean that either more current or longer counting times (or both) must be used to get statistically significant data. Longer counting times and higher currents lead to larger surface effects being produced over the course of the analysis. This may lead to changing counts on the various samples. Given that the Fe Lη (L_2–M_1 transition) has virtually the same character as that of the Ll line, their combination should not be critical. Even though the Fe Ll line has the lowest count rates out of the three possibilities being investigated (Lα, Lβ, and Ll lines), it appears to be the best X-ray line for quantitative EPMA at low voltage. Fialin et al. (1998) however, already made the prescient suggestion related to the transition metals, that "Despite their low intensities, the 'atomic' Ll-η peaks (3*s*-2*p* transition) are more convenient [than Lα-β] for those applications to [EPMA] practice."

While surface contamination effects are an important problem for soft X-ray EPMA, these effects seem to be small compared with the problems of anomalous X-ray emission and absorption and the proximity of the Lα and Lβ lines to the absorption edges. As mentioned above, one solution to overcome these difficulties is to use the Fe Ll line. However, currently none of the available EPMA software supports utilization of Fe Ll-η lines. For EPMA to advance to accuracy at low keV, particularly for the transition metals, Fe Ll-η lines should be used regularly and be supported in EPMA software. Once the Ll problem is remedied, the problems with surface effects and improper MACs can be addressed to refine the quantitative results for improved accuracy.

Conclusions

Currently one of the factors holding back full application of the low voltage, high spatial resolution EPMA (e.g., field emission EPMA) is the "energy barrier" raised by usage of the traditional X-ray analytical lines, e.g., Fe Kα. For optimal low voltage EPMA, there are many operational issues which must be fully addressed (e.g., clean vacuum; conductive coatings other than carbon; correct MACs). It has been demonstrated here that nontraditional lines such as Fe Ll-η can provide significant improvements in EPMA of Fe silicides at low voltages. Additionally, fully quantitative EPMA using standards with unnormalized totals must be utilized as the analytical total is a critical tool for quality control of microanalytical results. Nevertheless, understanding of the anomalies occurring from the most intense Fe Lα and Lβ X-ray emission lines would be useful to improve the reliability current matrix correction procedures.

Acknowledgments

Assistance with preparation of the Fe–Si samples was critical: E. Heikinheimo (Aalto University, Finland); Ridwan Sakidja and John Perepezko (UW Department of Material Science and Engineering); Veronica Berns, Rie Frederickson, and Daniel Fredrickson (UW Department of Chemistry); Phillipe Pinard (RWTH Aachen, Germany). Sample prep: Brian Hess and Travis Tenner (UW Department of Geoscience). Reviews by Christine Barszewski, Chloe Bonamici, Paul Carpenter, and an anonymous reviewer helped improve this article.

References

Anand, M., Taylor, L.A., Nazarov, M.A., Shu, J., Mao, H.K. & Hemley, R.J. (2004). Space weathering on airless planetary bodies: Clues from the lunar mineral hapkeite. *Proc Natl Acad Sci USA* **101**, 6847–6851.

Anderson, C.A. (1967). The quality of X-ray microanalysis in the ultra-soft X-ray region. *Br J Appl Phys* **18**, 1033–1043.

Armstrong, J. (2011). Low voltage and low overvoltage X-ray nanoanalysis with field emission electron microprobes and SEMs: Problems in quantitation for first-row transition elements. *2011 AGU Fall Meeting*, San Francisco, CA.

Castaing, R. (1951). Application of electron probes to local chemical and crystallographic analysis. Thesis, University of Paris, Publication *O.N.E.R.A*, No. 55.

Chantler, C.T., Olsen, K., Dragoset, R.A., Chang, J., Kishore, A.R., Kotochigova, S.A., Zucker, D.S. (2005). X-ray form factor, attenuation, and scattering tables. Available at www.nist.gov/pml/data/ffast/index.cfm.

Chopra, D. (1970). Ni L self-absorption spectrum. *Phys Rev A* **1**, 230–235.

Deslattes, R.D. (1969). Estimates of X-ray attenuation coefficients for the elements and their compounds. *Acta Cryst* **A25**, 89–93.

Deslattes, R.D., Kessler, E.G., Indelicato, P., DeBilly, L., Lindroth, E. & Anton, J. (2003). X-ray transition energies: New approach to a comprehensive evaluation. *Rev Mod Phys* **75**, 35–99.

Donovan, J.J., Kremser, D., Fournelle, J. & Goemann, K. (2012). *Probe for EPMA: Users Guide and Reference*. Available at ProbeSoftware.com.

Drouin, D., Couture, A.R., Joly, D., Tastet, X., Aimez, V. & Gauvin, R. (2007). CASINO V2.42: A fast and easy-to-use modeling tool for scanning electron microscopy and microanalysis users. *Scanning* **29**, 92–101.

Eisebitt, S. & Rubensson, J. (1994). Electronic structure of buried a-FeSi2 and B-FeSi2 layers. *Phys Rev B* **50**, 330–340.

Essene, E.J. & Fisher, D.C. (1986). Lightning strike fusion: Extreme reduction and metal-silicate liquid immiscibility. *Science* **234**, 189–193.

Fialin, M., Wagner, C., Metrich, N., Humler, E., Galoisy, L. & Bezos, A. (2001). Fe 3 + / ΣFe vs. FeLα peak energy for minerals and glasses: Recent advances with the electron microprobe. *Amer Mineral* **86**, 456–465.

Fialin, M., Wagner, C. & Remond, G. (1998). X-ray emission valence band spectrometry: Application to Cu and Fe L-series. *EMAS* **98**, 129–140.

Fischer, D.W. & Baun, W.L. (1967). Self-absorption effects in the soft X-Ray Mα and Mβ emission spectra of the rare earth elements. *J Appl Phys* **38**, 4830–4836.

Gopon, P., Fournelle, J. & Llovet, X. (2012). Soft X-ray EPMA of submicron phase lunar Fe–Si compounds. *Microsc Microanal* **18**(Suppl 2), 1728–1729.

Gopon, P., Sobol, P.E. & Fournelle, J. (2013). Random spectrometer motion for removal of time dependent artifacts in spectroscopy. *Microsc Microanal* **19**(Suppl 2), 814–815.

Heinrich, K.F.J. (1966). X-ray absorption uncertainty. In *The Electron Microprobe*, McKinley, T.D., Heinrich, K.F.J. & Wittry, D.B. (Eds.), pp. 296–377. New York: John Wiley & Sons.

Heinrich, K.F.J. (1987). Mass attenuation coefficients for electron microprobe microanalysis. In *Proc. 11th International Congress on X-Ray Optics and Microsanalysis*, London, Ontario, Canada, 1986, pp. 67–119.

Henke, B.L., Lee, P., Tanaka, T.J., Shimabukro, R.L. & Fijikawa, B.K. (1982). Low-energy X-ray interaction coefficients: Photoabsorption, scattering, and reflection: E = 100–2000 eV Z = 1–94. *Atomic Data Nucl Data Tables* **27**, 1–144.

Henke, B.L., White, R. & Lundberg, B. (1957). Semi-empirical determination of mass absorption coefficients for the 5 to 50 angstrom X-ray region. *J Appl Phys* **28**, 98–105.

Höfer, H.E. & Brey, G.P. (2007). The iron oxidation state of garnet by electron microprobe: Its determination with the flank method combined with major-element analysis. *Am Mineral* **92**, 873–885.

Kerur, B.R., Thontdarya, S.R. & Hanumaiah, B. (1993). X-ray attenuation coefficients at 6.46 keV and the validity of the mixture rule for compounds. *X-Ray Spectrom* **22**, 13–16.

Llovet, X., Heikinheimo, E., Núñez, A., Merlet, C., Almagro, J., Richter, S., Fournelle, J. & van Hoek, C. (2012). An inter-laboratory comparison of EPMA analysis of alloy steel at low voltage. In *IOP Conf Ser: Mater Sci Eng* **32**, 1–14.

Mackenzie, A.P. (1993). Recent progress in electron-probe microanalysis. *Rep Prog Phys* **56**, 557–604.

Ohnuma, I., Abe, S., Shimenouchi, S., Omori, T. & Kainuma, R. (2012). Experimental and thermodynamic studies of the Fe-Si binary system. *ISIJ Inte* **52**, 540–548.

Okamoto, H. (1990). Fe–Si (iron–silicon). In *Binary Alloy Phase Diagrams*, 2nd ed., Massalski, T.B. (Ed.), pp. 1771–1772. Materials Park, OH: ASM International.

O'Nions, R.K. & Smith, D.G.W. (1971). Investigation the $L_{II,\ III}$ emission spectra of Fe by electron microprobe: Part 2. The Fe $L_{II,\ III}$ spectra of Fe and Fe–Ti oxides. *Am Mineral* **56**, 1452–1455.

Pouchou, J.L. (1996). Use of soft X-rays in microanalysis. *Mikrochim Acta (Suppl)* **12**, 39–60.

Pouchou, J.L. & Pichoir, F. (1984). A new model for quantitative X-ray microanalysis. I.—application to the analysis of homogeneous samples. *Rech Aerosp* **3**, 167–192.

Pouchou, J.L., Pichoir, F. & Boivin, D. (1990). XPP procedure applied to quantitative EDS X-ray analysis in the SEM. In *Microbeam Analysis*, Michael, J.R. & Ingram, P. (Eds.), pp. 120–126. San Francisco, CA: San Francisco Press.

Rietmeijer, F., Nakamura, T., Tsuchiyama, A., Uesugi, K., Nakano, T. & Leroux, H. (2008). Origin and formation of iron silicide phases in the aerogel of the Stardust mission. *Meteoritics and Planet Sci* **1/2**, 121–134.

Ritchie, N.W.M. (2009). Spectrum simulation in DTSA-II. *Microsc Microanal* **15**, 454–468.

Sokaras, D., Kochur, A., Müller, M., Kolbe, M., Beckhoff, B., Mantler, M., Zarkadas, C., Andrianis, M., Lagoyannis, A. & Karydas, A. (2011). Cascade L-shell soft-X-ray emission as incident X-ray photons are tuned across the 1s ionization threshold. *Phys Rev A* **83**, 1–12.

Spicuzza, M.J., Valley, J.V., Fournelle, J., Huberty, J.M. & Treiman, A. (2011). Native silicon and Fe-silicides from the Apollo 16 lunar regolith: Extreme reduction, metal-silicate immiscibility, and shock melting. *42nd Lunar and Planet Sci Conf (2011)* **97**, 16–17.